NANO LETTERS

pubs.acs.org/NanoLett Letter

Converting the Bulk Transition Metal Dichalcogenides Crystal into Stacked Monolayers via Ethylenediamine Intercalation

Yeojin Ahn, Gyubin Lee, Namgyu Noh, Chulwan Lee, Duc Duy Le, Sunghun Kim, Yeonghoon Lee, Jounghoon Hyun, Chan-young Lim, Jaehun Cha, Mingi Jho, Seonggeon Gim, Jonathan D. Denlinger, Chan-Ho Yang, Jong Min Yuk, Myung Joon Han, and Yeongkwan Kim*

Cite This: *Nano Lett.* 2023, 23, 9733–9739 Read Online

ACCESS | Metrics & More | Article Recommendations

ABSTRACT: We report the synthesis of ethylenediamine-intercalated $NbSe_2$ and Li-ethylenediamine-intercalated $MoSe_2$ single crystals with increased interlayer distances and their electronic structures measured by means of angle-resolved photoemission spectroscopy (ARPES). X-ray diffraction patterns and transmission electron microscopy images confirm the successful intercalation and an increase in the interlayer distance. ARPES measurement reveals that intercalated $NbSe_2$ shows an electronic structure almost identical to that of monolayer $NbSe_2$. Intercalated $MoSe_2$ also returns the characteristic feature of the monolayer electronic structure, a direct band gap, which generates sizable photoluminescence even in the bulk form. Our results demonstrate that the properties and phenomena of the monolayer transition metal dichalcogenides can be achieved with large-scale bulk samples by blocking the interlayer interaction through intercalation.

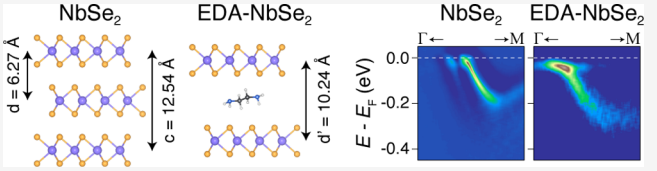

KEYWORDS: *transition metal dichalcogenides, $MoSe_2$, $NbSe_2$, intercalation, bulk, monolayer*

The physics of monolayer transition metal dichalcogenides (TMDs) is definitely one of the major research subjects of recent low-dimensional material science by virtue of its distinct properties that are not observed in their bulk counterparts.[1−3] For instance, in the case of group VI TMDs including $MoSe_2$, the transition from an indirect band gap to a direct band gap with decreasing thickness to a monolayer[4−9] greatly modifies the optical response of the system, which presents new avenues for optical devices.[10−13] Furthermore, owing to the noncentrosymmetric lattice structure of the monolayer, exotic electrical and optical responses associated with the Berry phase, curvature, and connection are enabled.[14−16] In the case of group V TMDs represented by 2H-$NbSe_2$, Ising superconductivity appears in the monolayer where the in-plane upper critical field is significantly enhanced, exceeding the Pauli paramagnetic limit, as a result of broken inversion symmetry of monolayer TMDs.[17−19]

In bulk TMDs, such physics of monolayer TMDs is hindered mainly due to the presence of interlayer coupling; the genuine electronic structure of the TMD layer with a direct band gap and with valley-dependent Berry curvature is either modified or canceled via interlayer coupling. The interlayer coupling generates the bonding and antibonding branches, and the number of branches depends on the number of layers, pushing the band top position at the Γ point and finally placing the valence band maximum (VBM) at the Γ point instead of the K point.[20] Alternating the stacking of layers in the bulk restores the inversion symmetry, canceling out any responses associated with the Berry phase, connection, or curvature.

The mechanism described above in turn suggests an alternative way to dig the hidden monolayer physics out of the bulk crystal rather than making it atomically thin. That is blocking the interlayer coupling, which can be achieved by simply enlarging the interlayer distance so that the wave functions at each layer do not overlap with one another. Practically, one straightforward approach is the intercalation of guest ions or molecules between the layers in TMDs. Indeed, there are several methods for intercalation, including the electrochemical method,[21,22] ion intercalation during vapor transport,[23,24] and immersion in a liquid solution.[25−27] Some results provide the recovery of monolayer physics in the bulk form as expected; however, the recovery of the genuine electronic structure of the TMD has not been fully addressed experimentally.

In this Letter, we report the recovered monolayer electronic structure in ethylenediamine ($C_2H_8N_2$, EDA)-intercalated

Received: June 18, 2023
Revised: October 6, 2023
Accepted: October 9, 2023
Published: October 30, 2023

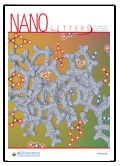

https://doi.org/10.1021/acs.nanolett.3c02268
Nano Lett. 2023, 23, 9733−9739

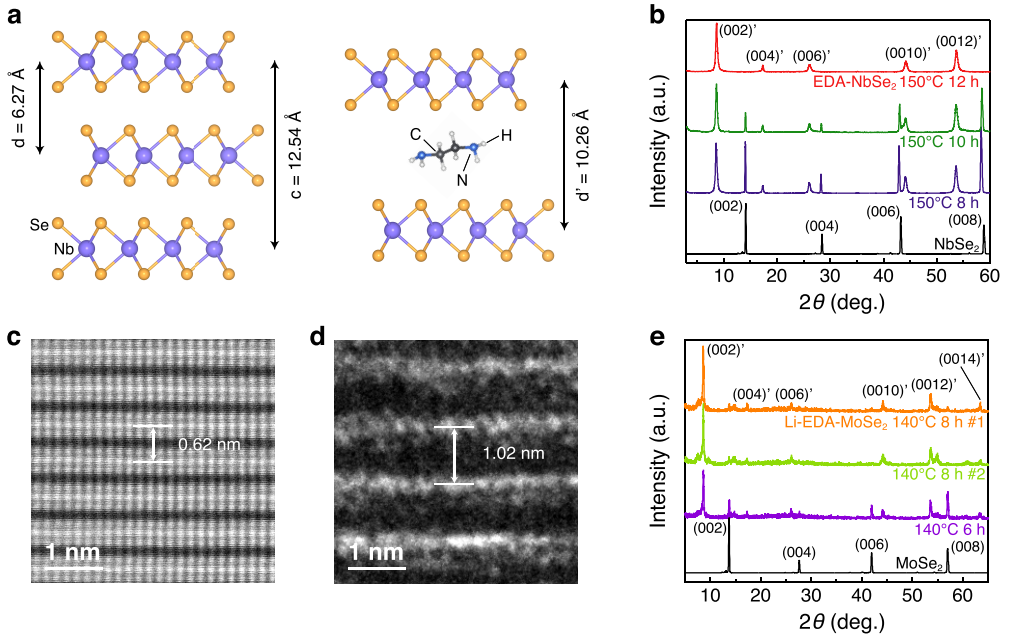

Figure 1. Schematic diagram of organic molecule intercalation and experimental data confirming intercalation. (a) Crystal structure of 2H-$NbSe_2$ (left) and EDA-intercalated $NbSe_2$ (right). (b) XRD spectra of pristine and EDA-intercalated $NbSe_2$. (c) HAADF-STEM image of pristine $NbSe_2$. (d) HRTEM image of intercalated $NbSe_2$. (e) XRD spectra of pristine and Li-EDA-intercalated $MoSe_2$.

$NbSe_2$ and Li-EDA-intercalated $MoSe_2$ in bulk forms with expanded interlayer distances (see Figure 1a). We confirmed that the intercalation successfully increases the interlayer distance to 10.26 Å through X-ray diffraction (XRD), transmission electron microscopy (TEM), and scanning electron microscopy (STEM). Angle-resolved photoemission spectroscopy (ARPES) was employed to investigate the electronic structure of intercalated crystals, which returns the genuine electronic structure of the monolayer TMD as expected for both $NbSe_2$ and $MoSe_2$. Finite photoluminescence (PL) from Li-EDA-intercalated $MoSe_2$ also verifies the formation of the direct band gap.

EDA was selected as the intercalant as it is in a stable charge-neutral form, avoiding interaction between the intercalant and the host materials, and has sufficient length to expand the interlayer distance to the extent of blocking the interlayer coupling. EDA was intercalated into TMD bulk crystals by immersion of single-crystal 2H-$NbSe_2$ in liquid EDA and 2H-$MoSe_2$ in a solution of Li metal dissolved in EDA. Two milliliters of an EDA or Li-EDA solution and 2−4 mg of 1 mm × 1 mm size single crystals were placed in a 10 mL borosilicate glass vial and sealed with a silicone cap and PTFE septum. We applied heat for 6−10 h by using reactor Monowave 50 and washed the sample with fresh EDA several times after removing the residual EDA or Li-EDA solution. All of the intercalation processes were performed in an argon-filled glovebox. TEM samples were prepared by using a focused ion beam (FIB) and measured by high-angle annular dark-field scanning transmission electron microscopy (HAADF-STEM) and high-resolution transmission electron microscopy (HRTEM). HAADF-STEM observation was performed with double Cs corrected Titan cubed G2 at an acceleration voltage of 300 kV (KARA, KAIST Analysis Center for Research Advancement). HRTEM observation was performed with a JEM-2100F electron microscope at an acceleration voltage of 200 kV. ARPES measurements were conducted at beamline 4.0.3 of the Advanced Light Source (ALS). Samples were cleaved at 10 K for pristine $MoSe_2$, $NbSe_2$, and intercalated $NbSe_2$ and at 100 K for intercalated $MoSe_2$ under ultrahigh vacuum with a pressure of $<4 \times 10^{-11}$ Torr. ARPES data of pristine and intercalated $NbSe_2$ are acquired with a photon energy of 55 eV. The photon energies utilized for measurements of pristine and intercalated $MoSe_2$ are 90 and 70 eV, respectively. The total energy resolution estimated with the reference gold spectrum was 27 meV or better. For first-principles density functional theory (DFT) calculation, the "Vienna ab initio simulation package"[28] was used on the basis of projector-augmented wave potential.[29] Within the Perdew−Burke−Ernzerhof type of GGA functional,[30] a Γ-centered k-grid of 20 × 20 × 6 and a plane-wave energy cutoff of 500 eV were adopted. The experimental lattice parameters are used for bulk calculations, and the internal coordinates are optimized with the force criterion of 0.01 eV/Å.

The XRD patterns of pristine and intercalated 2H-$NbSe_2$ samples under different heating conditions are shown in Figure 1b. The diffraction patterns of pristine $NbSe_2$ and EDA-intercalated $NbSe_2$ are indexed as a 2H-type $P6_3/mmc$ structure. New Bragg peaks first appear in the 150 °C 8 h sample, though original pristine $NbSe_2$ peaks are still present, which indicates a mixture of intercalated and non-intercalated regions. As a function of heating time, the intensity of newly emergent (pristine) peaks gradually increases (decreases). The pristine peaks disappear, and only new peaks remain in the 150 °C 12 h sample, suggesting rather uniform intercalation in the final stage. Lattice parameter c is estimated to be 12.54 Å for 2H-$NbSe_2$ and 20.52 Å for EDA-intercalated $NbSe_2$, indicating that the interlayer distance is increased from 6.27 to 10.26 Å.

A HAADF-STEM image of pristine $NbSe_2$ (Figure 1c) and a high-resolution TEM (HRTEM) image of intercalated $NbSe_2$ (Figure 1d) also confirm successful intercalation of EDA into $NbSe_2$; the distance between neighboring layers is enlarged compared to that of unintercalated bulk $NbSe_2$. Compared to the STEM image of pristine 2H $NbSe_2$, the HRTEM image of intercalated $NbSe_2$ appears to be fuzzy, presumably due to

https://doi.org/10.1021/acs.nanolett.3c02268
Nano Lett. 2023, 23, 9733−9739

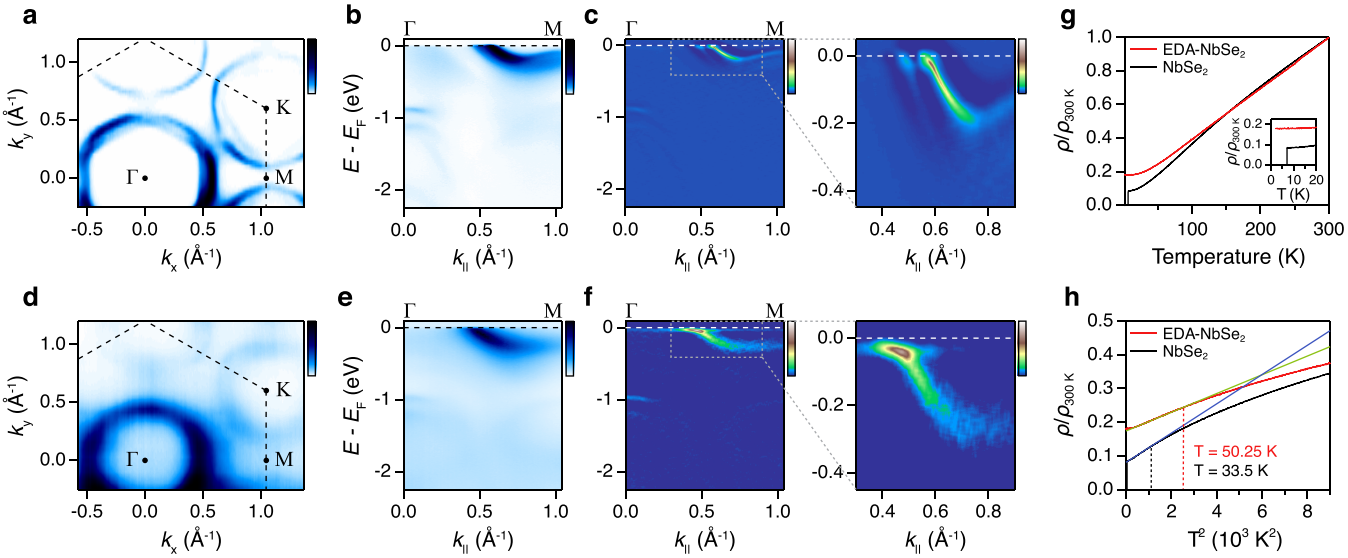

Figure 2. Electronic structure and resistivity of EDA-intercalated $NbSe_2$ compared with those of pristine bulk $NbSe_2$. ARPES data of unintercalated bulk $NbSe_2$ consist of (a) a Fermi surface map, (b) band dispersion along the Γ−M direction, and (c) a curvature plot of panel b and its magnified image. ARPES data of intercalated $NbSe_2$ consist of (d) a Fermi surface map, (e) band dispersion along the Γ−M direction, and (f) a curvature plot of panel e and its magnified image. (g) Temperature dependence of the electrical resistivity for pristine and intercalated samples. The bottom right inset shows a close-up for temperatures between 0 and 20 K. (h) Resistivity of pristine and intercalated $NbSe_2$ as a function of quadratic temperature. The blue and green lines are fits to $\rho = \rho_0 + AT^2$ (ρ_0 is the residual resistivity).

undesired deintercalation of EDA during the sample preparation process for TEM measurement and possible damage to the crystallinity by the intercalation of rather large organic molecules of EDA. The interlayer distance can be determined from the images, which coincides with the value estimated from XRD patterns. In the case of $MoSe_2$, Li is additionally introduced, along with EDA for intercalation. Other than co-intercalation of Li, the XRD patterns of intercalated samples prepared with different reaction times exhibit trends similar to those of $NbSe_2$; the intensity of pristine peaks decreases and the intensity of new peaks increases with the increased reaction time of the samples (Figure 1e). The interlayer distance is increased from 6.46 to 10.26 Å, which is also analogous to the case for EDA-intercalated $NbSe_2$. We note that EDA can be easily intercalated into metallic TMDs such as $NbSe_2$, whereas semiconducting $MoSe_2$ needs Li to be co-intercalated with EDA. Presumably, to enable the intercalation process, it would be necessary to align the electrochemical potential of EDA and the chemical potential of TMDs, and thus, an additional electron from Li should be introduced to fill the empty conduction state, which would not be necessary for metallic TMDs.[31]

Next, the electronic structure of intercalated TMD was measured by ARPES and compared with the bulk pristine case, which is summarized in Figure 2. The Fermi surface topology of pristine $NbSe_2$ presented in Figure 2a clearly shows two Nb 4d orbital-driven hexagonal pockets around the zone center and two trigonally warped pockets around the K point. Figure 2b shows band dispersion along the Γ−M high-symmetry line at the hexagonal Brillouin zone of pristine $NbSe_2$. Nb 4d-derived bands near the Fermi level are separated, which is the key feature generated by interlayer coupling.[32,33] This splitting is more clearly shown in Figure 2c, a curvature plot[34] in Figure 2b, and its magnified image on the right. The pancake-shaped band of Se $4p_z$ orbital origin is also observed (Figure 2b), but it is blurred presumably due to k_z broadening.[35−38]

The measured electronic structure of EDA-intercalated $NbSe_2$ is summarized in the same manner to directly compare with that of bulk pristine $NbSe_2$. The Fermi surface topology of the intercalated sample shown in Figure 2d is similar to that of pristine 2H-$NbSe_2$ with hole pockets at the Γ and K points, although it is blurred due to the possible damage from organic molecule intercalation. The intact Fermi surface topology confirms that the phase transition to the 1T structure through intercalation did not occur. Figure 2e shows band dispersion along the Γ−M direction. Nb 4d band splitting due to interlayer coupling is absent, sharply in contrast to the pristine bulk band dispersion (Figure 2c) where the bonding−antibonding splitting due to interlayer coupling is apparent. The curvature plot of Figure 2e and its enlarged image at the right (Figure 2f) confirm that the splitting of the Nb band near the Fermi level vanishes in the intercalated sample, presumably due to weakened interlayer coupling through intercalation, as expected. Indeed, the absence of band splitting coincides with the band structure of monolayer $NbSe_2$.[39−41]

The change in the electronic structure through EDA intercalation is also evidenced by the temperature-dependent electrical resistivity of bulk pristine and intercalated $NbSe_2$ shown in Figure 2g. As shown in the inset, the superconducting transition of bulk $NbSe_2$ occurs at ∼6 K, whereas EDA-intercalated $NbSe_2$ does not show any sudden decrease in resistivity down to 2 K. In addition, the overall power law dependence of resistivity on the temperature is modified, which suggests the landscape of charge density wave (CDW) transition and its fluctuation is also renormalized due to intercalation. Specifically, we estimated the point at which the temperature dependence of resistivity deviates from conventional $\sim T^2$, as the fluctuations of the CDW above the transition temperature are known to renormalize the carrier dynamics and thus the temperature dependence of resistivity.[42] As

https://doi.org/10.1021/acs.nanolett.3c02268
Nano Lett. 2023, 23, 9733−9739

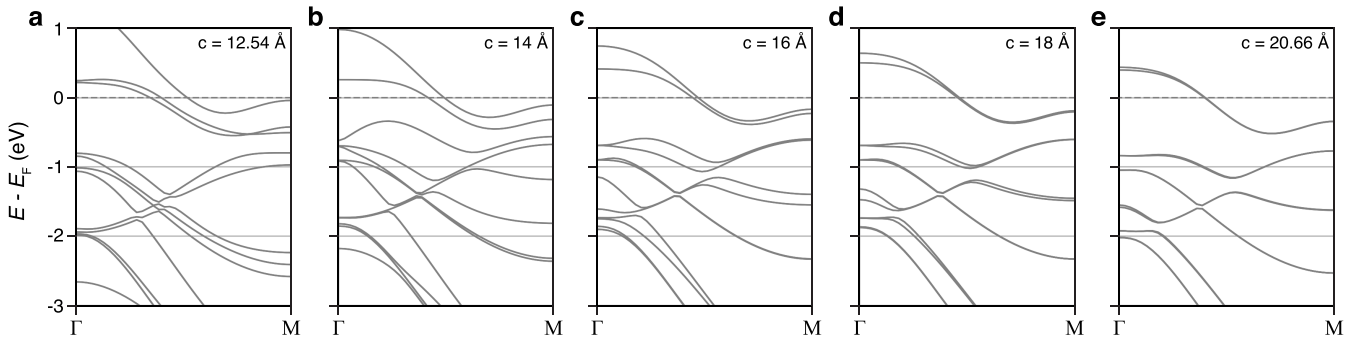

Figure 3. Calculated band structure of 2H-$NbSe_2$ with (a) the original c and (b−e) c values of ≤20.66 Å.

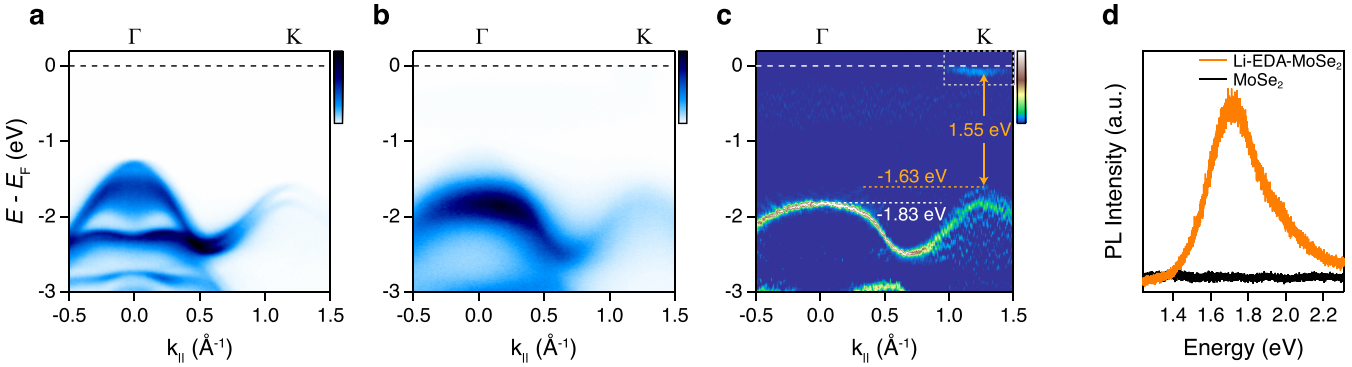

Figure 4. Direct band gap of Li-EDA-intercalated $MoSe_2$. Band dispersions of (a) pristine bulk $MoSe_2$ and (b) Li-EDA-intercalated $MoSe_2$ along the Γ−K direction. (c) Curvature plot of panel b. (d) PL spectra of pristine and intercalated $MoSe_2$.

indicated in Figure 2h, the temperature range showing T^2 behavior is increased from 33.5 K[43] of the original CDW transition temperature to ∼50.25 K, indicating an increased transition temperature similar to the case of electrochemically intercalated $NbSe_2$.[44]

To confirm that the observed change in the band structure is the result of diminished (enlarged) interlayer coupling (distance) via intercalation, DFT calculations of bulk 2H-$NbSe_2$ with an increasing lattice parameter c were carried out (Figure 3). The calculated band structures show that the key feature of bonding−antibonding splitting of the Nb 4d band near the Fermi level along the Γ−M direction is gradually diminished as lattice parameter c increases from the original $NbSe_2$ bulk value of 12.54 to 20.66 Å (Figure 3a). The band splits eventually become negligible, and the overall electronic structure is quite similar to that of the monolayer at c = 20.66 Å (Figure 3e). This finding supports our interpretation that the EDA intercalation mainly separates two adjacent $NbSe_2$ layers without changing other electronic properties. Note that in our DFT calculation, EDA intercalation is modeled by inserting a vacuum layer for the sake of simplicity into the calculation. Therefore, the good agreement between our DFT calculations and ARPES measurements demonstrates the role of EDA as a layer separator, enabling us to effectively investigate the monolayer limit in the bulk form of the sample.

The recovery of the genuine electronic structure of TMD through intercalation is also reproduced in the case of Li-EDA-intercalated $MoSe_2$. ARPES spectra of the Li-EDA-intercalated sample compared with the bulk pristine sample are presented in Figure 4a−c. Band dispersion of bulk $MoSe_2$ along the Γ−K direction (Figure 4a) shows that the VBM is located at the Γ point, driven by orbital hybridization, with valence band branches of bonding and antibonding states dominated by transition metal 4d and chalcogen p_z orbital character. The electronic structure of Li-EDA-intercalated $MoSe_2$ shown in Figure 4b retains a 2H-type band topology without a phase transition to the 1T structure, coinciding with the XRD result. Figure 4b shows the Γ−K band dispersion of the intercalated sample. Although the ARPES spectra are blurred, presumably due to the developed inhomogeneity of the system through intercalation, it is noticeable that the number of branches of the valence band near the zone center of the intercalated sample is reduced. The curvature plot of the original ARPES spectra of the intercalated sample for improved visualization (Figure 4c) shows that the valence band at the Γ point has only one branch, and the top of the valence band is lower than that at the K point, resulting in the VBM being shifted to the K point. The VBM at the K point is ∼200 meV higher than the valence band top at the Γ point. In addition, the conduction band is also observed by the donation of charge from the intercalation of the alkali metal Li into the sample. The conduction band minimum also turned out to be located at the K point, combined with the VBM at the K point. This leads to a direct band gap of ∼1.55 eV, which is a characteristic feature of the monolayer $MoSe_2$ electronic structure.[8]

After confirmation of the recovery of the monolayer electronic structure, the PL responses of the pristine bulk sample and intercalated sample are measured to investigate the formation of the direct band gap separately through the optical response. As expected, the pristine $MoSe_2$ sample does not exhibit PL.[12] In sharp contrast to the bulk case, the PL peak emerges for EDA-intercalated $MoSe_2$, centered at ∼1.7 eV. We note that the observed PL is not attributed to the Li-EDA. The absorption spectrum of Li-EDA exhibits a peak at 0.99 eV,[45] which is far smaller than the observed energy scale of the PL peak. Hence, returning a sizable PL peak indicates the

https://doi.org/10.1021/acs.nanolett.3c02268
Nano Lett. 2023, 23, 9733−9739

formation of a direct band gap. However, the intensity of the PL peak is not comparable to that from monolayer $MoSe_2$ in the previous studies, which is likely limited by the damage on the crystal introduced by intercalation. Also, the energy scale of PL peaks of ~1.7 eV is larger than previous PL results of monolayer $MoSe_2$[12,13] and captured the direct band gap size in our study (Figure 4c). One possible origin would be the internal strain caused by intercalation as the renormalization of the band gap size upon biaxial compressive strain to MoS_2 has been previously reported,[46] and the intercalation of organic molecules in an inhomogeneous manner can lead to local internal strain and possibly increase the band gap. Another possible origin is the decrease in PL intensity of the A exciton and the increase in intensity of the B exciton due to Se vacancies.[47] The creation of bands within the band gap caused by Se vacancies can affect the exciton recombination process to favor recombination via a lower spin−orbit split valence band at K corresponding to the B exciton.

In conclusion, we were able to synthesize EDA-intercalated $NbSe_2$ and Li-EDA-intercalated $MoSe_2$ single crystals with increased interlayer distances and confirmed that the interlayer interaction is weakened enough to transform the bulk crystals into stacked individual monolayers through direct electronic structure diagnostics. Overall, both $NbSe_2$ and $MoSe_2$ exhibit monolayer-like band dispersion and optical properties after intercalation, the absence of bonding−antibonding splitting leading to the direct band gap in the $MoSe_2$ case. We believe the impact of this success should be broad as the intercalation can be generally applied to the various van der Waals (vdW) materials; it could allow us to access the pure two-dimensional physics without undesired interlayer interaction such as the cases of $RuCl_3$,[48−51] Kagome,[52−56] and van der Waals magnets.[57−60] Practically, securing monolayer properties with large-scale bulk samples could greatly reduce the hurdles in device fabrication for application.

AUTHOR INFORMATION

Corresponding Author

Yeongkwan Kim − *Department of Physics, Korea Advanced Institute of Science and Technology, Daejeon 34141, Republic of Korea;* orcid.org/0000-0003-1408-0550; Phone: +82-42-350-2516; Email: yeongkwan@kaist.ac.kr

Authors

Yeojin Ahn − *Department of Physics, Korea Advanced Institute of Science and Technology, Daejeon 34141, Republic of Korea;* orcid.org/0000-0001-5688-5707

Gyubin Lee − *Department of Physics, Korea Advanced Institute of Science and Technology, Daejeon 34141, Republic of Korea*

Namgyu Noh − *Department of Materials Science and Engineering, Korea Advanced Institute of Science and Technology, Daejeon 34141, Republic of Korea;* orcid.org/0000-0002-0427-3757

Chulwan Lee − *Department of Physics, Korea Advanced Institute of Science and Technology, Daejeon 34141, Republic of Korea*

Duc Duy Le − *Department of Physics, Korea Advanced Institute of Science and Technology, Daejeon 34141, Republic of Korea*

Sunghun Kim − *Department of Physics, Ajou University, Suwon 16499, Republic of Korea;* orcid.org/0000-0001-9320-7243

Yeonghoon Lee − *Quantum Spin Team, Korea Research Institute of Standards and Science, Daejeon 34113, Republic of Korea*

Jounghoon Hyun − *Department of Physics, Korea Advanced Institute of Science and Technology, Daejeon 34141, Republic of Korea;* orcid.org/0000-0003-2254-4984

Chan-young Lim − *Department of Physics, Korea Advanced Institute of Science and Technology, Daejeon 34141, Republic of Korea*

Jaehun Cha − *Department of Physics, Korea Advanced Institute of Science and Technology, Daejeon 34141, Republic of Korea*

Mingi Jho − *Department of Physics, Korea Advanced Institute of Science and Technology, Daejeon 34141, Republic of Korea*

Seonggeon Gim − *Department of Physics, Korea Advanced Institute of Science and Technology, Daejeon 34141, Republic of Korea*

Jonathan D. Denlinger − *Advanced Light Source, Lawrence Berkeley National Laboratory, Berkeley, California 94720, United States*

Chan-Ho Yang − *Department of Physics, Korea Advanced Institute of Science and Technology, Daejeon 34141, Republic of Korea;* orcid.org/0000-0002-3384-4272

Jong Min Yuk − *Department of Materials Science and Engineering, Korea Advanced Institute of Science and Technology, Daejeon 34141, Republic of Korea;* orcid.org/0000-0002-4677-7363

Myung Joon Han − *Department of Physics, Korea Advanced Institute of Science and Technology, Daejeon 34141, Republic of Korea;* orcid.org/0000-0002-8089-7991

Complete contact information is available at: https://pubs.acs.org/10.1021/acs.nanolett.3c02268

Author Contributions

Y.K. conceived the project. Y.A. synthesized bulk pristine and intercalated single crystals and conducted XRD and PL measurements. ARPES data were measured by Y.A., G.L., S.K., Y.L., C.-y.L., J.H., J.C., M.J., S.G., J.D.D., and Y.K. Y.A., S.K., and Y.K. analyzed the ARPES data. N.N. and J.M.Y. performed TEM measurements. C.L. and M.J.H. performed DFT calculations. D.D.L. and C.-H.Y. carried out resistance measurements. Y.A. and Y.K. wrote the manuscript with contributions from all authors.

Notes

The authors declare no competing financial interest.

ACKNOWLEDGMENTS

This work was supported by the National Research Foundation of Korea via Grants 2021R1A2C1013119, 2017R1A3B1023686, 2020R1A4A2002828, and 2022K1A3A1A25081713, funded by the Ministry of Science and ICT of the Republic of Korea. This work was also supported by National Measurement Standard Services and Technical Services for SME funded by Korea Research Institute of Standards and Science (KRISS-2023-GP2023-0015). The work at Ajou University was supported by the National Research Foundation of Korea, funded by the Ministry of Education (2021R1A6A1A10044950) and the Ministry of Science and ICT (RS-2023-00210828). Use of the Advanced Light Source, Lawrence Berkeley National Laboratory, is supported by the Office of Basic Energy Sciences of the U.S. Department of Energy under Contract DE-AC02-

https://doi.org/10.1021/acs.nanolett.3c02268
Nano Lett. 2023, 23, 9733−9739

05CH11231. The authors acknowledge KAIST Analysis Center for Research Advancement (KARA) for XRD and PL measurement facilities.

REFERENCES

(1) Butler, S. Z.; Hollen, S. M.; Cao, L.; Cui, Y.; Gupta, J. A.; Gutiérrez, H. R.; Heinz, T. F.; Hong, S. S.; Huang, J.; Ismach, A. F.; Johnston-Halperin, E.; Kuno, M.; Plashnitsa, V. V.; Robinson, R. D.; Ruoff, R. S.; Salahuddin, S.; Shan, J.; Shi, L.; Spencer, M. G.; Terrones, M.; Windl, W.; Goldberger, J. E. Progress, Challenges, and Opportunities in Two-Dimensional Materials Beyond Graphene. *ACS Nano* **2013**, *7* (4), 2898−2926.

(2) Manzeli, S.; Ovchinnikov, D.; Pasquier, D.; Yazyev, O. V.; Kis, A. 2D transition metal dichalcogenides. *Nat. Rev. Mater.* **2017**, *2* (8), 17033.

(3) Wang, Q. H.; Kalantar-Zadeh, K.; Kis, A.; Coleman, J. N.; Strano, M. S. Electronics and optoelectronics of two-dimensional transition metal dichalcogenides. *Nat. Nanotechnol.* **2012**, *7* (11), 699−712.

(4) Zhu, Z. Y.; Cheng, Y. C.; Schwingenschlögl, U. Giant spin-orbit-induced spin splitting in two-dimensional transition-metal dichalcogenide semiconductors. *Phys. Rev. B* **2011**, *84* (15), No. 153402.

(5) Kumar, A.; Ahluwalia, P. K. Electronic structure of transition metal dichalcogenides monolayers 1H-MX_2 (M = Mo, W; X = S, Se, Te) from ab-initio theory: new direct band gap semiconductors. *Eur. Phys. J. B* **2012**, *85* (6), 186.

(6) Cheiwchanchamnangij, T.; Lambrecht, W. R. L. Quasiparticle band structure calculation of monolayer, bilayer, and bulk MoS_2. *Phys. Rev. B* **2012**, *85* (20), No. 205302.

(7) Jin, W.; Yeh, P.-C.; Zaki, N.; Zhang, D.; Sadowski, J. T.; Al-Mahboob, A.; van der Zande, A. M.; Chenet, D. A.; Dadap, J. I.; Herman, I. P.; Sutter, P.; Hone, J.; Osgood, R. M. Direct Measurement of the Thickness-Dependent Electronic Band Structure of MoS_2 Using Angle-Resolved Photoemission Spectroscopy. *Phys. Rev. Lett.* **2013**, *111* (10), No. 106801.

(8) Zhang, Y.; Chang, T.-R.; Zhou, B.; Cui, Y.-T.; Yan, H.; Liu, Z.; Schmitt, F.; Lee, J.; Moore, R.; Chen, Y.; Lin, H.; Jeng, H.-T.; Mo, S.-K.; Hussain, Z.; Bansil, A.; Shen, Z.-X. Direct observation of the transition from indirect to direct bandgap in atomically thin epitaxial $MoSe_2$. *Nat. Nanotechnol.* **2014**, *9* (2), 111−115.

(9) Mo, S.-K.; Hwang, C.; Zhang, Y.; Fanciulli, M.; Muff, S.; Hugo Dil, J.; Shen, Z.-X.; Hussain, Z. Spin-resolved photoemission study of epitaxially grown $MoSe_2$ and WSe_2 thin films. *J. Phys.: Condens. Matter* **2016**, *28* (45), No. 454001.

(10) Splendiani, A.; Sun, L.; Zhang, Y.; Li, T.; Kim, J.; Chim, C.-Y.; Galli, G.; Wang, F. Emerging Photoluminescence in Monolayer MoS_2. *Nano Lett.* **2010**, *10* (4), 1271−1275.

(11) Mak, K. F.; Lee, C.; Hone, J.; Shan, J.; Heinz, T. F. Atomically Thin MoS_2: A New Direct-Gap Semiconductor. *Phys. Rev. Lett.* **2010**, *105* (13), No. 136805.

(12) Tongay, S.; Zhou, J.; Ataca, C.; Lo, K.; Matthews, T. S.; Li, J.; Grossman, J. C.; Wu, J. Thermally Driven Crossover from Indirect toward Direct Bandgap in 2D Semiconductors: $MoSe_2$ versus MoS_2. *Nano Lett.* **2012**, *12* (11), 5576−5580.

(13) Tonndorf, P.; Schmidt, R.; Böttger, P.; Zhang, X.; Börner, J.; Liebig, A.; Albrecht, M.; Kloc, C.; Gordan, O.; Zahn, D. R. T.; Michaelis de Vasconcellos, S.; Bratschitsch, R. Photoluminescence emission and Raman response of monolayer MoS_2, $MoSe_2$, and WSe_2. *Opt. Express* **2013**, *21* (4), 4908−4916.

(14) Cao, T.; Wang, G.; Han, W.; Ye, H.; Zhu, C.; Shi, J.; Niu, Q.; Tan, P.; Wang, E.; Liu, B.; Feng, J. Valley-selective circular dichroism of monolayer molybdenum disulphide. *Nat. Commun.* **2012**, *3* (1), 887.

(15) Cho, S.; Park, J.-H.; Hong, J.; Jung, J.; Kim, B. S.; Han, G.; Kyung, W.; Kim, Y.; Mo, S. K.; Denlinger, J. D.; Shim, J. H.; Han, J. H.; Kim, C.; Park, S. R. Experimental Observation of Hidden Berry Curvature in Inversion-Symmetric Bulk 2*H*−WSe_2. *Phys. Rev. Lett.* **2018**, *121* (18), No. 186401.

(16) Son, J.; Kim, K.-H.; Ahn, Y. H.; Lee, H.-W.; Lee, J. Strain Engineering of the Berry Curvature Dipole and Valley Magnetization in Monolayer MoS_2. *Phys. Rev. Lett.* **2019**, *123* (3), No. 036806.

(17) Xi, X.; Wang, Z.; Zhao, W.; Park, J.-H.; Law, K. T.; Berger, H.; Forró, L.; Shan, J.; Mak, K. F. Ising pairing in superconducting $NbSe_2$ atomic layers. *Nat. Phys.* **2016**, *12* (2), 139−143.

(18) Xing, Y.; Zhao, K.; Shan, P.; Zheng, F.; Zhang, Y.; Fu, H.; Liu, Y.; Tian, M.; Xi, C.; Liu, H.; Feng, J.; Lin, X.; Ji, S.; Chen, X.; Xue, Q.-K.; Wang, J. Ising Superconductivity and Quantum Phase Transition in Macro-Size Monolayer $NbSe_2$. *Nano Lett.* **2017**, *17* (11), 6802−6807.

(19) de la Barrera, S. C.; Sinko, M. R.; Gopalan, D. P.; Sivadas, N.; Seyler, K. L.; Watanabe, K.; Taniguchi, T.; Tsen, A. W.; Xu, X.; Xiao, D.; Hunt, B. M. Tuning Ising superconductivity with layer and spin−orbit coupling in two-dimensional transition-metal dichalcogenides. *Nat. Commun.* **2018**, *9* (1), 1427.

(20) Fang, S.; Kuate Defo, R.; Shirodkar, S. N.; Lieu, S.; Tritsaris, G. A.; Kaxiras, E. Ab initio tight-binding Hamiltonian for transition metal dichalcogenides. *Phys. Rev. B* **2015**, *92* (20), No. 205108.

(21) Morales, J.; Santos, J.; Tirado, J. L. Electrochemical studies of lithium and sodium intercalation in $MoSe_2$. *Solid State Ionics* **1996**, *83* (1), 57−64.

(22) Li, X.-L.; Li, Y.-D. MoS_2 Nanostructures: Synthesis and Electrochemical Mg^{2+} Intercalation. *J. Phys. Chem. B* **2004**, *108* (37), 13893−13900.

(23) Somoano, R. B.; Hadek, V.; Rembaum, A. Alkali metal intercalates of molybdenum disulfide. *J. Chem. Phys.* **1973**, *58* (2), 697−701.

(24) Dresselhaus, M. S.; Dresselhaus, G. Intercalation compounds of graphite. *Adv. Phys.* **2002**, *51* (1), 1−186.

(25) Toh, M. L.; Tan, K. J.; Wei, F. X.; Zhang, K. K.; Jiang, H.; Kloc, C. Intercalation of organic molecules into SnS_2 single crystals. *J. Solid State Chem.* **2013**, *198*, 224−230.

(26) Hatakeda, T.; Noji, T.; Kawamata, T.; Kato, M.; Koike, Y. New Li-Ethylenediamine-Intercalated Superconductor $Li_x(C_2H_8N_2)_yFe_{2-z}Se_2$ with T_c = 45 K. *J. Phys. Soc. Jpn.* **2013**, *82* (12), No. 123705.

(27) Márkus, B. G.; Szirmai, P.; Kollarics, S.; Náfrádi, B.; Forró, L.; Chacón-Torres, J. C.; Pichler, T.; Simon, F. Improved Alkali Intercalation of Carbonaceous Materials in Ammonia Solution. *Phys. Status Solidi B* **2019**, *256* (12), No. 1900324.

(28) Kresse, G.; Furthmüller, J. Efficient iterative schemes for ab initio total-energy calculations using a plane-wave basis set. *Phys. Rev. B* **1996**, *54* (16), 11169−11186.

(29) Kresse, G.; Joubert, D. From ultrasoft pseudopotentials to the projector augmented-wave method. *Phys. Rev. B* **1999**, *59* (3), 1758−1775.

(30) Perdew, J. P.; Burke, K.; Ernzerhof, M. Generalized Gradient Approximation Made Simple. *Phys. Rev. Lett.* **1996**, *77* (18), 3865−3868.

(31) Chhowalla, M.; Shin, H. S.; Eda, G.; Li, L.-J.; Loh, K. P.; Zhang, H. The chemistry of two-dimensional layered transition metal dichalcogenide nanosheets. *Nat. Chem.* **2013**, *5* (4), 263−275.

(32) Johannes, M. D.; Mazin, I. I.; Howells, C. A. Fermi-surface nesting and the origin of the charge-density wave in $NbSe_2$. *Phys. Rev. B* **2006**, *73* (20), No. 205102.

(33) Calandra, M.; Mazin, I. I.; Mauri, F. Effect of dimensionality on the charge-density wave in few-layer 2*H*−$NbSe_2$. *Phys. Rev. B* **2009**, *80* (24), No. 241108.

(34) Zhang, P.; Richard, P.; Qian, T.; Xu, Y.-M.; Dai, X.; Ding, H. A precise method for visualizing dispersive features in image plots. *Rev. Sci. Instrum.* **2011**, *82* (4), No. 043712.

(35) Inosov, D. S.; Zabolotnyy, V. B.; Evtushinsky, D. V.; Kordyuk, A. A.; Büchner, B.; Follath, R.; Berger, H.; Borisenko, S. V. Fermi surface nesting in several transition metal dichalcogenides. *New J. Phys.* **2008**, *10* (12), No. 125027.

(36) Shen, D. W.; Zhang, Y.; Yang, L. X.; Wei, J.; Ou, H. W.; Dong, J. K.; Xie, B. P.; He, C.; Zhao, J. F.; Zhou, B.; Arita, M.; Shimada, K.; Namatame, H.; Taniguchi, M.; Shi, J.; Feng, D. L. Primary Role of the

https://doi.org/10.1021/acs.nanolett.3c02268
Nano Lett. 2023, 23, 9733−9739

Barely Occupied States in the Charge Density Wave Formation of $NbSe_2$. *Phys. Rev. Lett.* **2008**, *101* (22), No. 226406.
(37) Borisenko, S. V.; Kordyuk, A. A.; Zabolotnyy, V. B.; Inosov, D. S.; Evtushinsky, D.; Büchner, B.; Yaresko, A. N.; Varykhalov, A.; Follath, R.; Eberhardt, W.; Patthey, L.; Berger, H. Two Energy Gaps and Fermi-Surface "Arcs" in $NbSe_2$. *Phys. Rev. Lett.* **2009**, *102* (16), No. 166402.
(38) Rossnagel, K.; Seifarth, O.; Kipp, L.; Skibowski, M.; Voß, D.; Krüger, P.; Mazur, A.; Pollmann, J. Fermi surface of 2*H*−$NbSe_2$ and its implications on the charge-density-wave mechanism. *Phys. Rev. B* **2001**, *64* (23), No. 235119.
(39) Ugeda, M. M.; Bradley, A. J.; Zhang, Y.; Onishi, S.; Chen, Y.; Ruan, W.; Ojeda-Aristizabal, C.; Ryu, H.; Edmonds, M. T.; Tsai, H.-Z.; Riss, A.; Mo, S.-K.; Lee, D.; Zettl, A.; Hussain, Z.; Shen, Z.-X.; Crommie, M. F. Characterization of collective ground states in single-layer $NbSe_2$. *Nat. Phys.* **2016**, *12* (1), 92−97.
(40) Nakata, Y.; Sugawara, K.; Ichinokura, S.; Okada, Y.; Hitosugi, T.; Koretsune, T.; Ueno, K.; Hasegawa, S.; Takahashi, T.; Sato, T. Anisotropic band splitting in monolayer $NbSe_2$: implications for superconductivity and charge density wave. *npj 2D Mater. Appl.* **2018**, *2* (1), 12.
(41) Xu, C.-Z.; Wang, X.; Chen, P.; Flötotto, D.; Hlevyack, J. A.; Lin, M.-K.; Bian, G.; Mo, S.-K.; Chiang, T.-C. Experimental and theoretical electronic structure and symmetry effects in ultrathin $NbSe_2$ films. *Phys. Rev. Mater.* **2018**, *2* (6), No. 064002.
(42) Bhoi, D.; Khim, S.; Nam, W.; Lee, B. S.; Kim, C.; Jeon, B.-G.; Min, B. H.; Park, S.; Kim, K. H. Interplay of charge density wave and multiband superconductivity in 2*H*-Pd_xTaSe_2. *Sci. Rep.* **2016**, *6* (1), 24068.
(43) Xi, X.; Zhao, L.; Wang, Z.; Berger, H.; Forró, L.; Shan, J.; Mak, K. F. Strongly enhanced charge-density-wave order in monolayer $NbSe_2$. *Nat. Nanotechnol.* **2015**, *10* (9), 765−769.
(44) Zhang, H.; Rousuli, A.; Zhang, K.; Luo, L.; Guo, C.; Cong, X.; Lin, Z.; Bao, C.; Zhang, H.; Xu, S.; Feng, R.; Shen, S.; Zhao, K.; Yao, W.; Wu, Y.; Ji, S.; Chen, X.; Tan, P.; Xue, Q.-K.; Xu, Y.; Duan, W.; Yu, P.; Zhou, S. Tailored Ising superconductivity in intercalated bulk $NbSe_2$. *Nat. Phys.* **2022**, *18* (12), 1425−1430.
(45) Zurek, E. Alkali Metals in Ethylenediamine: Alkali Metals in Ethylenediamine: A Computational Study of the Optical Absorption Spectra and NMR Parameters of $[M(en)_3^{\delta+}\cdot M^{\delta-}]$ Ion Pairs. *J. Am. Chem. Soc.* **2011**, *133* (13), 4829−4839.
(46) Hui, Y. Y.; Liu, X.; Jie, W.; Chan, N. Y.; Hao, J.; Hsu, Y.-T.; Li, L.-J.; Guo, W.; Lau, S. P. Exceptional Tunability of Band Energy in a Compressively Strained Trilayer MoS_2 Sheet. *ACS Nano* **2013**, *7* (8), 7126−7131.
(47) Iberi, V.; Liang, L.; Ievlev, A. V.; Stanford, M. G.; Lin, M.-W.; Li, X.; Mahjouri-Samani, M.; Jesse, S.; Sumpter, B. G.; Kalinin, S. V.; Joy, D. C.; Xiao, K.; Belianinov, A.; Ovchinnikova, O. S. Nanoforging Single Layer $MoSe_2$ Through Defect Engineering with Focused Helium Ion Beams. *Sci. Rep.* **2016**, *6* (1), 30481.
(48) Sarikurt, S.; Kadioglu, Y.; Ersan, F.; Vatansever, E.; Aktürk, O. Ü.; Yüksel, Y.; Akıncı, Ü.; Aktürk, E. Electronic and magnetic properties of monolayer α-$RuCl_3$: a first-principles and Monte Carlo study. *Phys. Chem. Chem. Phys.* **2018**, *20* (2), 997−1004.
(49) Du, L.; Huang, Y.; Wang, Y.; Wang, Q.; Yang, R.; Tang, J.; Liao, M.; Shi, D.; Shi, Y.; Zhou, X.; Zhang, Q.; Zhang, G. 2D proximate quantum spin liquid state in atomic-thin α-$RuCl_3$. *2D Materials* **2019**, *6* (1), No. 015014.
(50) Tian, Y.; Gao, W.; Henriksen, E. A.; Chelikowsky, J. R.; Yang, L. Optically Driven Magnetic Phase Transition of Monolayer $RuCl_3$. *Nano Lett.* **2019**, *19* (11), 7673−7680.
(51) Lee, J.-H.; Choi, Y.; Do, S.-H.; Kim, B. H.; Seong, M.-J.; Choi, K.-Y. Multiple spin-orbit excitons in α-$RuCl_3$ from bulk to atomically thin layers. *npj Quantum Mater.* **2021**, *6* (1), 43.
(52) Lin, Y.-P.; Nandkishore, R. M. Complex charge density waves at Van Hove singularity on hexagonal lattices: Haldane-model phase diagram and potential realization in the kagome metals AV_3Sb_5 (A = K, Rb, Cs). *Phys. Rev. B* **2021**, *104* (4), No. 045122.
(53) Park, T.; Ye, M.; Balents, L. Electronic instabilities of kagome metals: Saddle points and Landau theory. *Phys. Rev. B* **2021**, *104* (3), No. 035142.
(54) Wu, X.; Schwemmer, T.; Müller, T.; Consiglio, A.; Sangiovanni, G.; Di Sante, D.; Iqbal, Y.; Hanke, W.; Schnyder, A. P.; Denner, M. M.; Fischer, M. H.; Neupert, T.; Thomale, R. Nature of Unconventional Pairing in the Kagome Superconductors AV_3Sb_5 (A = K, Rb, Cs). *Phys. Rev. Lett.* **2021**, *127* (17), No. 177001.
(55) Denner, M. M.; Thomale, R.; Neupert, T. Analysis of Charge Order in the Kagome Metal AV_3Sb_5 (A = K, Rb, Cs). *Phys. Rev. Lett.* **2021**, *127* (21), No. 217601.
(56) Kim, S.-W.; Oh, H.; Moon, E.-G.; Kim, Y. Monolayer Kagome metals AV_3Sb_5. *Nat. Commun.* **2023**, *14* (1), 591.
(57) Huang, B.; Clark, G.; Navarro-Moratalla, E.; Klein, D. R.; Cheng, R.; Seyler, K. L.; Zhong, D.; Schmidgall, E.; McGuire, M. A.; Cobden, D. H.; Yao, W.; Xiao, D.; Jarillo-Herrero, P.; Xu, X. Layer-dependent ferromagnetism in a van der Waals crystal down to the monolayer limit. *Nature* **2017**, *546* (7657), 270−273.
(58) Li, T.; Jiang, S.; Sivadas, N.; Wang, Z.; Xu, Y.; Weber, D.; Goldberger, J. E.; Watanabe, K.; Taniguchi, T.; Fennie, C. J.; Fai Mak, K.; Shan, J. Pressure-controlled interlayer magnetism in atomically thin CrI_3. *Nat. Mater.* **2019**, *18* (12), 1303−1308.
(59) Bedoya-Pinto, A.; Ji, J.-R.; Pandeya, A. K.; Gargiani, P.; Valvidares, M.; Sessi, P.; Taylor, J. M.; Radu, F.; Chang, K.; Parkin, S. S. P. Intrinsic 2D-XY ferromagnetism in a van der Waals monolayer. *Science* **2021**, *374* (6567), 616−620.
(60) Kim, K.; Lim, S. Y.; Lee, J.-U.; Lee, S.; Kim, T. Y.; Park, K.; Jeon, G. S.; Park, C.-H.; Park, J.-G.; Cheong, H. Suppression of magnetic ordering in XXZ-type antiferromagnetic monolayer $NiPS_3$. *Nat. Commun.* **2019**, *10* (1), 345.

https://doi.org/10.1021/acs.nanolett.3c02268
Nano Lett. 2023, 23, 9733−9739